P6.6 **NUMERICAL SIMULATION OF CELL INTERACTION**

Brian F. Jewett* and Robert B. Wilhelmson
Dept. of Atmospheric Sciences & NCSA
University of Illinois at Urbana-Champaign

Bruce D. Lee
Dept. of Earth Sciences
University of Northern Colorado, Greeley

1. INTRODUCTION

The behavior of isolated thunderstorm cells has been extensively explored through numerical simulation, including the relationship between cell intensity and longevity and the local buoyancy and shear. Observations have indicated that cell propagation and intensity may be further modulated by interaction with nearby cells. The interaction may be fostered by differing propagation characteristics as a result of mesoscale boundaries, cell age, splitting, and/or rotational properties. Interaction can be destructive, as occurs when one storm interrupts the inflow to another, or constructive, as if one cell intercepts and strengthens along the outflow boundary of another.

We are studying idealized cell interaction[2]. This work was motivated by radar observations of cell morphology during the 19 April 1996 tornado outbreak affecting Illinois and nearby states. Cell splitting and merging was common early in the outbreak, and further analysis (Lee et al. 2000) revealed that cell merging preceded many of the tornado events on this day. Earlier studies (e.g. Wolf and Szoke 1996) found cell intensification upon collocation of a leading cell's rear-flank gust front with the forward flank of a nearby trailing storm. We have undertaken this study to explore, through numerical simulation, the behavior of and interaction between convective cells.

2. METHODOLOGY

The numerical simulations were carried out in an idealized, horizontally uniform framework. The environment was based on a sounding extracted from an earlier 3-km MM5 study of the tornado outbreak (Jewett et al. 2000). This model sounding originated near the time (late afternoon) and location (north-eastern Missouri) of convective initiation along the drytrough in the MM5 simulation. The sounding was characterized by significant instability (3400 J kg^{-1}) and a nearly straight hodograph (Fig. 1).

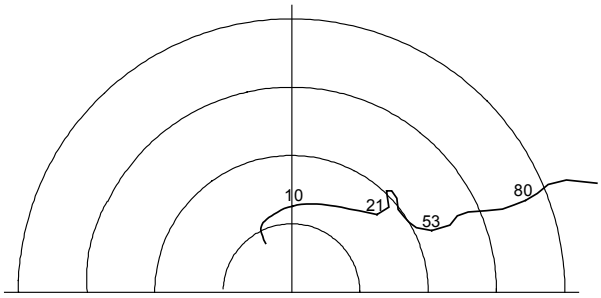

Fig.1: Initial wind profile. Speed rings are every 10 m s^{-1}. Heights along hodograph are in (km * 10).

The simulations were carried out using an early (1.2β) version of the Weather Research and Forecasting model (WRF; Michalakes et al. 2001). Given the preproduction nature of the model, a simple configuration was chosen, with warm rain microphysics and 2nd-order diffusion employed. 1 km horizontal resolution and 60 vertical levels were used within a 90x90x20 km domain. Two thermals, with 3 and 2K temperature perturbations, were placed at the initial time. The 3K cell was located at the domain center, while the 2K cell placement was varied within a 30x30 km region about the initial cell position. In addition, two control runs (with only a single 3K or 2K thermal) were made to evaluate unperturbed cell behavior.

The matrix of simulations is depicted in Fig. 2. The markers indicate the initial positions of the 2K ("secondary") cell relative to the 3K ("primary") one. Secondary cell positions were spaced every 2.5 km over the 30x30 km area, with an additional, offset mesh within $\pm$10 km. The mesh defined a total of 232 simulations in addition to the two control cases.

[1] *Corresponding author address:*
Dr. Brian F. Jewett
212 Atmos Sci Bldg,
105 S. Gregory St., Urbana, IL 61801
email: jewett@atmos.uiuc.edu

[2] Online at redrock.ncsa.uiuc.edu/~jewett/SLS02

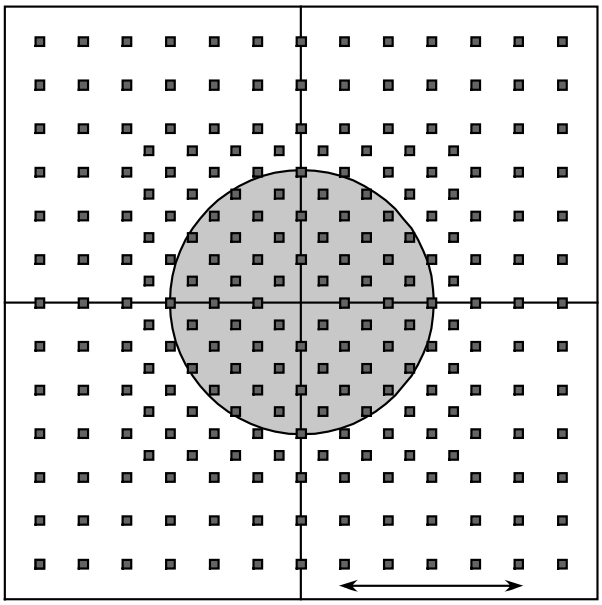

Fig. 2: Simulation matrix. The black squares represent the initial secondary cell locations (the primary 3K cell is always at the center). Arrow denotes a 10 km distance. This figure represents initial cell positions (at ±15 km), not the 90x90 km model domain. Shaded R=7.5 km circle represents the region over which initial thermals overlapped.

While no secondary cell was collocated at the origin (defining a single 5K perturbation), the simulation mesh did include thermals placed closely enough to make cell distinction difficult. The WRF temperature perturbations varied as $\theta' \sim cos(R)$ for R up to 8500 m. The 7.5-km radius circle in Fig. 2 and later figures defines the approximate distance at which the center 3K temperature perturbation was reduced by 1/e. Visual inspection of early rainwater structure showed initial cells to be separate at 10 km distance and progressively less distinct at distances under 7.5 km. Superimposed thermals may be meaningful for modeling closely-spaced cells in a line but may be less relevant in terms of model behavior at 1 km resolution.

3. CELL MORPHOLOGY

Each simulation was run for 2.5 hours. Data was saved at 1 minute intervals. Statistics were gathered on peak surface, 1 and 4 km vertical vorticity; 1 km and overall peak updraft speed, and maximum surface wind speed. In addition, because the 1996 outbreak was characterized by significant (up to low-F3 intensity) but generally short-lived tornadoes, the surface vorticity field maxima were tracked to establish their vorticity *duration*, the time over which individual vorticity maxima exceeded 0.01, 0.015 or 0.020 s^{-1}. These statistics were contoured and displayed in the same form as Fig. 2. In the limiting case of no base state flow and no boundary effects with two identical (e.g. 3K) thermals, we would expect axisymmetric results, with any cell orientation (with one at center) producing the same results as another for the same cell spacing. The wind profile (Fig. 1), different initial thermal magnitudes (the 3K cell intensifies and splits more quickly), thermal discretization (cell centers between grid points) and possibly boundary effects will break this symmetry.

The peak surface vorticity over all cases was sorted and is shown in Fig. 3. Vorticity values hereafter are scaled by 10^4. Among all runs, a wide range of surface rotation is indicated, with values ranging from 200 to nearly 500 (0.02 to nearly 0.05 s^{-1}). We note that the control cases, with 3K and 2K (single-cell) undisturbed thermals, reached 352 and 305, respectively. Thus, most cases of cell interaction were destructive, with a narrow range of cell orientations leading to greater surface rotation than in their undisturbed counterparts.

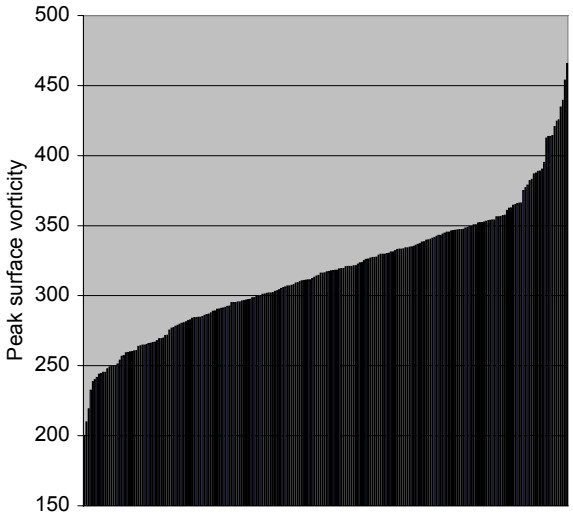

Fig. 3: Peak vertical vorticity maxima (x10^{-4} s^{-1}) for all 232 cases, displayed in ascending order.

The same vorticity statistics are contoured relative to their initial (Fig. 2) cell orientation in Fig. 4. Overlapping or closely spaced cells are one configuration resulting in higher rotation. A prominent asymmetry exists along a northeast-southwest axis. Secondary cells initially southwest of the primary cell lead to greater vorticity, while the opposite orientation is clearly weaker. Values for the southwest case are higher than the 3K control, while that to the northeast are notably lower than the 2K control.

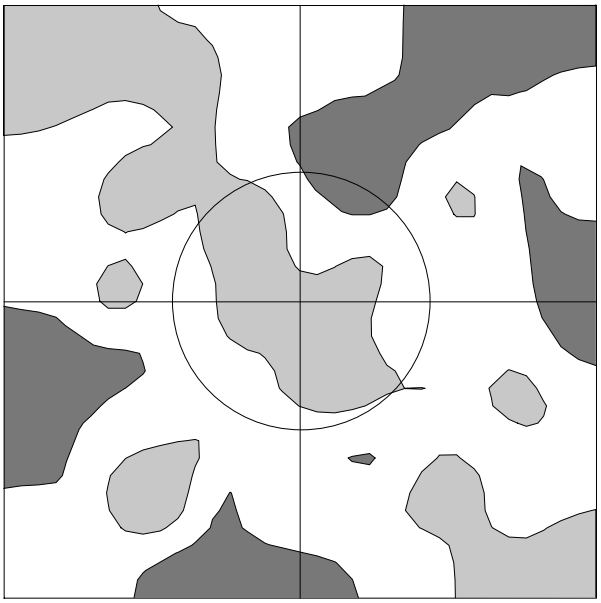

Fig. 4: Peak vertical vorticity maxima, contoured at their initial cell locations as in Fig. 2. Shading represents values over 340 (light) or under 280 (dark, $x10^{-4}$ s^{-1}).

We note also that the vorticity time series maxima were often highly peaked. Such short duration and significant (above their time mean) maxima were not expected at 1 km resolution. Two types of time filtering were employed to reduce sampling errors (of maxima falling between 1-minute data sets). The results (not shown) were very similar to that in Fig. 4.

The vorticity duration values were similarly sorted and appear in Fig. 5. This represents the longest time period during which surface vorticity maxima were above a selected (150, or .015 s^{-1}) threshold. A wide range, from 10 to nearly 75 minutes, was indicated. The control values were 66 and 64 minutes for 3K and 2K cells, again suggesting that only a narrow range of cell orientation exceeded the control results. The horizontal dependence (Fig. 6) has similarities to Fig. 4. Cases for which the secondary cell was initially southwest of the primary were divided into longer and shorter duration rotation, even in the region (Fig. 4) in which strong rotation was indicated. Shorter duration times were a consequence of delayed development (and the 2.5 hour simulation cutoff) accompanying adjacent split cell interaction, or a tendency to line out as the western cell's forward flank downdraft intensified.

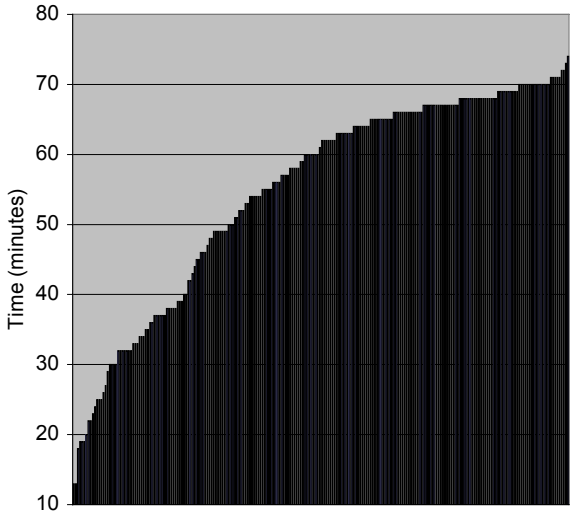

Fig. 5: Vorticity duration time (minutes) for all cases, at a threshold of 150.

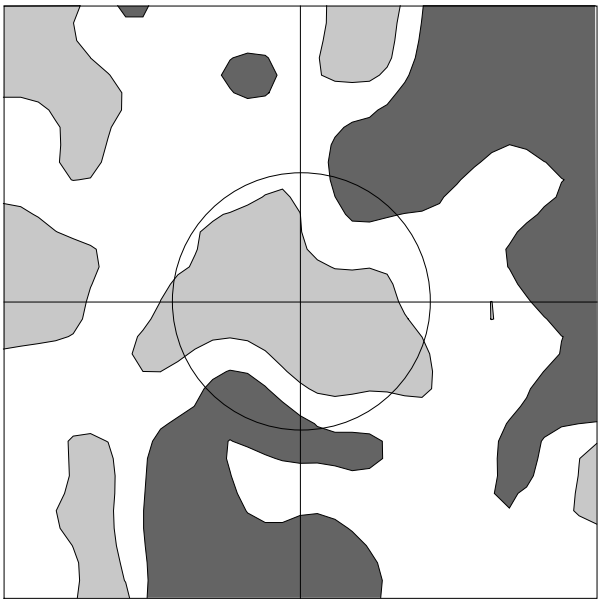

Fig. 6: Vertical vorticity duration for vorticity exceeding 150 $x10^{-4}$ s^{-1}. Shading represents times over 64 min (light) or under 48 min (dark).

It is possible that some of the sensitivity seen above is also reflected in or connected to primary updraft strength. The distribution of peak vertical velocity (Fig. 7) suggests that this is not the case. The variation among simulations is not particularly large, ranging from 54 to 70 m s^{-1}. Note the narrow difference (2 m s^{-1}) distinguishing shaded regions in the figure.

A distinct pattern exists within the 7.5 km radius, suggesting unique behavior for adjacent, developing cells. The north-south and east-west symmetry suggests (1) the initial 1K θ' difference did not affect peak updraft strength and (2) the east-west configuration was less favored (resulted in more linear structure).

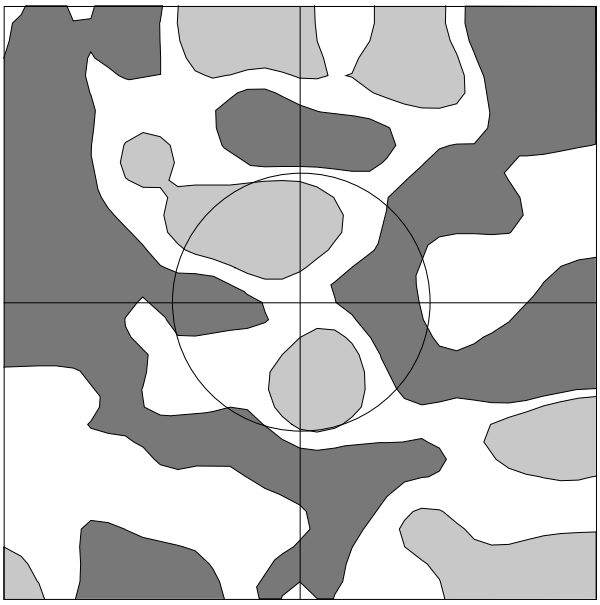

Fig. 7: Horizontal map of peak updraft intensity. Light shading identifies regions in which updraft strength was $\geq$ 62 m s^{-1}, while dark shading indicates updrafts of $\leq$ 60 m s^{-1}.

Beyond the close-cell radius, the pattern is less clear. Perhaps most notable is the lack of intensity difference between the region of stronger rotation (second cell southwest of first) and weaker rotation (northeast offset) seen in Fig. 4. The scatter plot of peak (or 1 km) updraft strength vs. maximum surface vorticity (not shown) has no clear pattern, other than the prevalence of strong (60 m s^{-1} updrafts), moderately rotating cells in the experimental results.

The relationship between peak surface rotation and duration is illustrated in Fig. 8. The clustering of values near T=70 minutes is likely a consequence of the simulation cutoff at 2.5 hours. It is significant that such a wide range of rotational properties can be realized under identical instability and shear profiles as a consequence of cell interaction. The relationship between initial orientation and cell rotational intensity, duration and morphology will be investigated further.

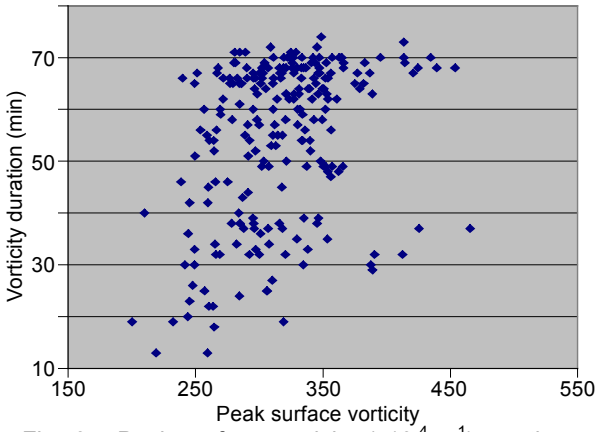

Fig. 8: Peak surface vorticity (x10^{-4} s^{-1}) vs. time period when surface vorticity exceeds 150 x10^{-4} s^{-1}.

4. FUTURE WORK

These results are preliminary and further analysis is underway. Higher resolution simulations with prognostic turbulence kinetic energy, delayed cell initiation, and ice microphysics are planned for this and other MM5 model soundings. Beyond these goals, a more general study over a range of idealized profiles of instability and shear will let us extend this work beyond our specific case.

5. ACKNOWLEDGEMENTS

This work was supported by NSF under grant ATM-9986672. Computing and other support was provided by the National Center for Supercomputing Applications.

6. REFERENCES

Jewett, B. F., B. D. Lee and R. B. Wilhelmson, 2000: Initiation and evolution of severe convection in the 19 April 1996 Illinois tornado outbreak. *Preprints, 20th Conf. on Severe Local Storms*, Orlando, 74-77.

Lee, B. D., B. F. Jewett and R. B. Wilhelmson, 2000: Supercell differentiation and organization for the 19 April 1996 Illinois tornado outbreak. *Preprints, 20th Conf. on Severe Local Storms*, Orlando, 222-225.

Michalakes, J., S. Chen, J. Dudhia, L. Hart, J. Klemp, J. Middlecoff and W. Skamarock, 2001: "Development of a next generation regional weather research and forecast model" in *Developments in Teracomputing*: Proceedings of the 9th ECMWF Workshop on the Use of High Performance Computing in Meteorology. (www.mmm.ucar.edu/mm5/mpp/ecmwf01.htm)

Wolf, R., and E. Szoke, 1996: A multiscale analysis of the 21 July 1993 northeast Colorado tornadoes. *Preprints, 18th Conf. on Severe Local Storms*, Amer. Meteor. Soc., San Francisco, 403-407.